Cerebral Cortex, September 2017;27: 4523–4536

doi: 10.1093/cercor/bhw257
Advance Access Publication Date: 6 September 2016
Original Article

ORIGINAL ARTICLE

Imagined and Executed Actions in the Human Motor System: Testing Neural Similarity Between Execution and Imagery of Actions with a Multivariate Approach

Adam Zabicki[1], Benjamin de Haas[2,3], Karen Zentgraf [4,5], Rudolf Stark[5], Jörn Munzert[1], and Britta Krüger[1,5]

[1]Institute for Sports Science, Justus Liebig University Giessen, Giessen, 35394, Germany, [2]Institute of Cognitive Neuroscience, University College London, London, WC1H 0AP, UK, [3]Experimental Psychology, University College London, London, WC1H 0AP, UK, [4]Institute of Sport and Exercise Sciences, University of Münster, Münster, 48149, Germany, and [5]Bender Institute of Neuroimaging, Justus Liebig University Giessen, Giessen, 35394, Germany

Address correspondence to Adam Zabicki, Institute for Sport Science, Justus Liebig University Giessen, Kugelberg 62, 35394 Giessen, Germany. Email: adam.zabicki@sport.uni-giessen.de.

Abstract

Simulation theory proposes motor imagery (MI) to be a simulation based on representations also used for motor execution (ME). Nonetheless, it is unclear how far they use the same neural code. We use multivariate pattern analysis (MVPA) and representational similarity analysis (RSA) to describe the neural representations associated with MI and ME within the frontoparietal motor network. During functional magnetic resonance imaging scanning, 20 volunteers imagined or executed 3 different types of right-hand actions. Results of MVPA showed that these actions as well as their modality (MI or ME) could be decoded significantly above chance from the spatial patterns of BOLD signals in premotor and posterior parietal cortices. This was also true for cross-modal decoding. Furthermore, representational dissimilarity matrices of frontal and parietal areas showed that MI and ME representations formed separate clusters, but that the representational organization of action types within these clusters was identical. For most ROIs, this pattern of results best fits with a model that assumes a low-to-moderate degree of similarity between the neural patterns associated with MI and ME. Thus, neural representations of MI and ME are neither the same nor totally distinct but exhibit a similar structural geometry with respect to different types of action.

Key words: action mapping, functional equivalence, motor imagery, MVPA, RSA

Introduction

During the last 20 years, motor simulation phenomena have become a major topic in the field of cognitive neuroscience. Within this discussion, Jeannerod (2001) formulated his mental simulation theory. This theory proposes a functional equivalence between simulating and executing an action. More precisely, it argues that every action involves a covert stage, and that this covert state includes the goal of the action and its environmental consequences. Jeannerod and Frak (1999) concluded that these covert actions are also actions—the only difference being that they are not executed. One prominent situation corresponding to these so-called covert actions is the conscious, self-intended simulation of one's own actions, that is, motor imagery (MI).

On a neural level, it has been proposed that MI is a simulation based on motor representations in the brain (Jeannerod

2001). This has been supported by several neuroimaging studies showing that roughly the same brain areas are involved in both motor execution (ME) and MI (Decety et al. 1994; Deiber et al. 1996; Porro et al. 1996; Lotze et al. 1999; Guillot et al. 2008; Hanakawa et al. 2008; Munzert et al. 2009). However, most of these studies used traditional forms of functional magnetic resonance imaging (fMRI) data analysis (Decety et al. 1994; Stephan et al. 1995; Deiber et al. 1996; Porro et al. 1996; Lotze et al. 1999; Ehrsson et al. 2003; Lorey et al. 2013) and indicate only overall activity changes in brain regions in response to a stimulus or a cognitive task (Friston et al. 1995). Such analyses do not consider more distributed changes of activation patterns within a given brain site, which may occur in the absence of overall amplitude modulations. Newer approaches such as multivariate decoding (Haxby et al. 2001; Haynes and Rees 2005; Kamitani and Tong 2005; Kriegeskorte, 2011) allow the investigation of the representational content of neuronal population codes. These approaches interpret stimulus-related activity patterns as distributed representations of the stimuli. One aim of these newer approaches is to identify such distributed response patterns in order to link them to a given stimulus or a specific experimental condition.

The potential of these studies to answer open questions within the field of motor simulation phenomena was demonstrated recently in a couple of studies using multivariate pattern analysis (MVPA). For example, it has been shown that these analysis techniques allow the decoding of intended, imagined, and executed types of hand actions from parietal and frontal motor areas (Gallivan et al. 2011a, 2011b, 2013; Oosterhof et al. 2012a; Pilgramm et al. 2016) as well as from lateral occipitotemporal cortex (Oosterhof et al. 2012b; Pilgramm et al. 2016). Furthermore, it has been demonstrated that distributed neural response patterns in motor and motor-related areas can be used to distinguished whether they were elicited by the execution, imagery (Park et al. 2015), or observation of a hand action (Filimon et al. 2015). A recent study by Pilgramm et al. (2016) provided evidence that patterns of activity within motor, premotor, and posterior parietal cortex (PPC) differentiate between 3 different types of imagined hand actions: a force production task, an aiming task, and an extension–flexion task.

This study examines the similarity between neural activation patterns for different imagined and executed hand actions in the same sample. In our fMRI experiment, subjects worked on 6 experimental conditions and 1 baseline condition. In the experimental conditions, they had to either imagine or execute 3 different right-hand actions: aiming, extension–flexion, and squeezing (Lorey et al. 2013; Pilgramm et al. 2016). We then decoded the *type* (aiming vs. extension–flexion vs. squeezing) and *modality* (MI vs. ME) of imagined and executed hand actions based on the spatial patterns of BOLD signals they evoked in motor, premotor, and posterior parietal cortices. Separate multivariate classifiers were trained and tested for each region of interest (ROI) in order to obtain an index of pattern discriminability. In the second step, we decoded across the 2 modalities (MI and ME) to test whether MI and the execution of specific hand movements share a similar neural code. Third, we applied a representational similarity analysis (RSA) (Kriegeskorte et al. 2008) to characterize the representational geometry of MI and ME conditions in every motor region via representational dissimilarity matrices (RDMs) (Kriegeskorte et al. 2008; Kriegeskorte and Kievit 2013). Finally, we compared the respective RDMs with several predicted RDMs based on different computational models: an action type model, an action modality model, and 3 different mixed models (Kriegeskorte 2009; Khaligh-Razavi and Kriegeskorte 2014). In general, we used different multivariate methods to deepen the understanding of neural representations of MI and ME.

Materials and Methods

Subjects

Twenty right-handed volunteers [14 female, mean age = 22.9 years, standard deviation (SD) = 2.9] with normal or corrected-to-normal vision participated in this experiment. They reported no history of psychiatric or neurological disorders, and no history or current use of any psychoactive medication. The study was approved by the local Ethics Committee of the Psychology and Sport Science Department of the Justus Liebig University Giessen, and all subjects gave informed written consent in accordance with the Declaration of Helsinki. The study took place at the Bender Institute of Neuroimaging (BION, Justus Liebig University).

Design and Task

The experiment consisted of 3 imagery conditions, 3 execution conditions, and 1 rest condition. Before the fMRI experimental phase, subjects completed a familiarization session (see Familiarization Session). In the imagery and execution conditions, they were instructed to either imagine or execute one of the 3 tasks: 1) a force production task squeezing bellows, (2) an aiming task pointing with the index finger at 5 targets affixed to the bellows, or (3) an extension–flexion movement with the right hand (i.e., the fingers) alongside the bellows (Fig. 1*a*). The aiming task required no memorizing of a spatial sequence of targets, because subjects were instructed to simply imagine pointing to 5 affixed targets one after another (Lorey et al. 2014; Pilgramm et al. 2016). Thus, in total, subjects were scanned during 7 conditions. During the imagery and rest conditions, subjects kept their eyes closed; otherwise, they kept them open to receive visual feedback. Conditions were presented in a pseudorandomized order counterbalanced across subjects. Each trial started with a written instruction presented for 2.5 s ("Imagine Squeezing Hand," "Imagine Aiming Hand," "Imagine Rhythmic Movement Hand," "Execute Squeezing Hand," "Execute Aiming Hand," "Execute Rhythmic Movement Hand," or "Close Your Eyes and Rest") followed by a jitter [0 – 90% of time of repetition (TR)] and the respective imagery, execution, or rest phase (8 s; Fig. 1*b*). Instructions were presented with a PC running Presentation software (Neurobehavioral Systems) and projected onto a screen behind the scanner that could be viewed through a mirror attached to the head coil. During imagery and rest, subjects kept their eyes closed, reopening them only when the MI or rest phase was finished. This was signaled by a sound. After each trial, subjects were asked to rate (maximum 3 s) the perceived quality of their imagery or execution performance on a 7-point scale ranging from "very high" (7) to "very low" (1). For the imagery task, quality is reflected by the perceived vividness of the mental image of the respective movement; for the execution task, quality is reflected by a perceived correct performance of the respective movement. The rating also occurred after the rest trial in order to keep the stimulation as well as the motor performance of the subjects similar in each trial and experimental condition. Here, participants were instructed to rate how well they did relax. Each subject performed 10 runs of 14 trials each (corresponding to 2 trials in each of the 7 conditions) in each of the 2

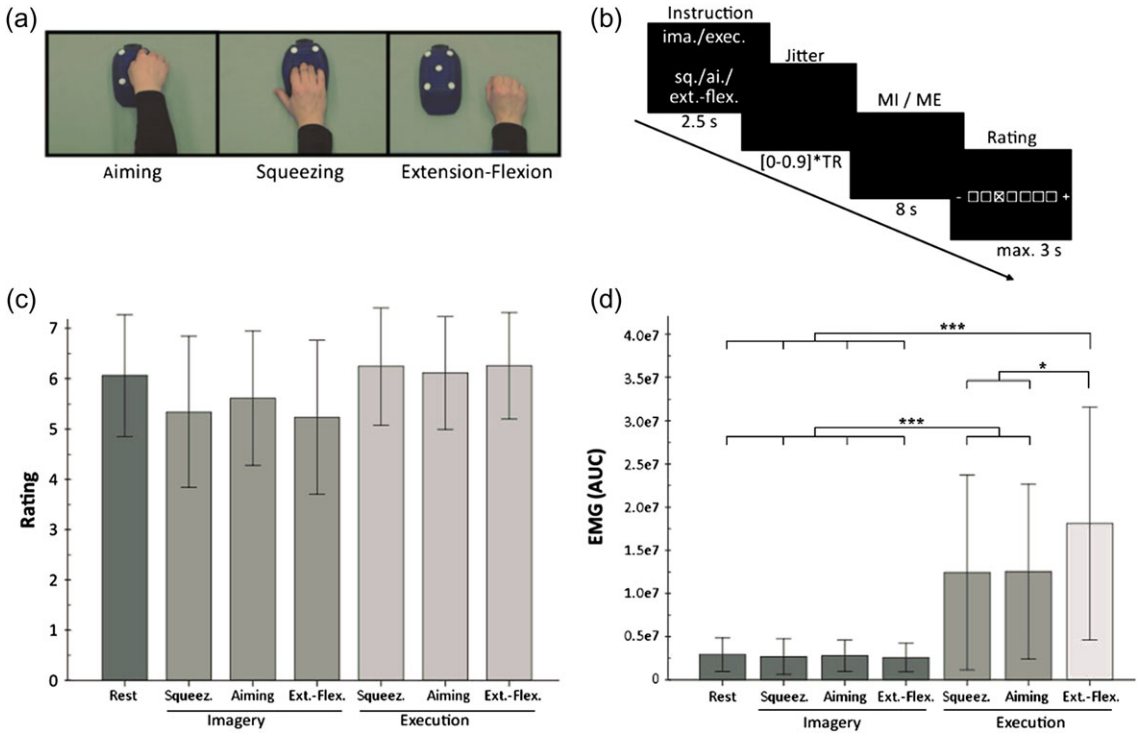

Figure 1. (*a*) Experimental conditions and (*b*) temporal structure of the experiment. (*c*) Subjective rating of the perceived quality of performance of participants: Bars and error bars show means ±1 standard error of the mean (SEM). (*d*) EMG data: Means ±1 SEM of the "area under the curve." Asterisks indicate statistical significance of *t* tests between the experimental conditions. *P < 0.05, ***P < 0.001, adjusted for multiple testing using the Holm–Bonferroni method.

separate scanning sessions within 1 week, amounting to a total of 20 runs, 280 trials, and a scanning time of approximately 80 min. To control for involuntary movements during MI as well as the performance during ME trials, we recorded the surface electromyographic (EMG) sum potential from 2 target muscles of the right forearm during scanning (*M. flexor carpi radialis, M. palmaris longus*).

Familiarization Session

Prior to the first fMRI-scanning session, subjects completed a preparatory session to familiarize themselves with the different experimental conditions and the experimental setting. First, they observed and executed the different movements (see earlier) before imagining them. All subjects were trained to imagine the different hand movements in a first person perspective. More precisely, participants were instructed to imagine the movements as if they were performing it, including kinesthetic as well as visual aspects of the movement. We used MATLAB (MathWorks Inc.) to simulate the forthcoming fMRI session and monitored EMG signals from several target muscles of the right forearm using a real-time biofeedback system (Biofeedback 2000 x-pert, Schuhfried GmbH). This procedure allowed us to give subjects feedback on whether they performed MI without any notable muscle contraction. After each training trial, subjects rated the quality of their imagery on a 7-point scale ranging from very high (7) to very low (1). This session lasted a total of 30 min.

Image Acquisition and Preprocessing

The fMRI data were collected on a 3-T whole-body scanner (Siemens Prisma) with a standard 20-channel head coil. We acquired 1 structural image from each participant consisting of 176 T1-weighted sagittal images (1-mm slice thickness; MPRAGE) at the first session and a fieldmap [40 slices; time of echo (TE)(1): 10 ms; TE(2): 12.46 ms; TR: 1000 ms] for the separate scanning sessions. For the run of functional imaging, a total of 1,820 volumes were registered using a T2*-weighted gradient echo-planar imaging sequence with 40 slices covering the whole brain (slice thickness = 3 mm; 0.75 mm gap; descending; time of acquisition = 2.4375 s; TR = 2.5 s; TE = 30 ms; flip angle = 87 degrees; field of view = 192 mm × 192 mm). The orientation of the axial slices was parallel to the AC–PC line. Trial onsets were jittered within 0–90 % of the TR.

Image preprocessing was carried out using SPM 12 (Wellcome Department of Imaging Neuroscience, University College London, UK). Origin coordinates were adjusted to the anterior commissure. Furthermore, realignment and unwarping were performed using voxel displacement maps generated from the fieldmaps (Hutton et al. 2002), and the functional images were coregistered with the anatomical scan for the respective subject. Smoothing was executed with an isotropic 3-dimensional Gaussian filter with a full-width-at-half-maximum (FWHM) kernel of 5 mm.

Data Analysis

Regions of Interest

The anatomical scan was used to reconstruct the cortical surface of each hemisphere using FreeSurfer (http://surfer.nmr.mgh.harvard.edu). ROIs were selected on the basis of previous findings reported in the MI literature (Grèzes and Decety 2001; Jeannerod 2001; Ehrsson et al. 2003; Heed et al. 2011) and defined anatomically on an individual basis using the FreeSurfer

parcellation algorithm (Destrieux et al. 2010; cf. Pilgramm et al. 2016). We defined 7 ROIs per hemisphere as follows:

1. Primary motor cortex (M1), defined as the precentral gyrus.
2. Dorsal and ventral premotor cortex (dPMC and vPMC), defined as the superior and inferior part of the precentral sulcus, respectively.
3. Superior (SPL) and inferior parietal lobule (IPL), defined as the supramarginal and the angular gyrus as well as the intraparietal sulcus (IPS) including transverse parietal sulci.
4. Primary auditory cortex (A1), defined as the anterior transverse temporal gyrus (Shapleske et al. 1999), and frontomarginal gyrus (FMG) serving as control regions

Defining ROIs on an individual basis allowed us to work with high anatomical precision and avoided the need for spatial normalization.

General Linear Models

A first-level analysis was computed with SPM 12 using separate general linear models (GLMs) for each subject and each of the 20 runs. We created 7 boxcar regressors corresponding to the 7 conditions. The boxcar functions of each regressor spanned the imagery, execution, or rest interval (i.e., 8 s). Each regressor was convoluted with a canonical hemodynamic response function. Moreover, 6 movement parameters from the rigid-body transformation of the motion-correction procedure were entered as covariates in the GLM. The voxel-based time series were filtered with a high-pass filter (time constant = 128 s). Based on these GLMs, we calculated 6 contrast images per subject and run, each contrasting one of the MI or ME conditions with the rest condition.

Multivariate Pattern Analysis

The purpose of the MVPA was to analyze whether the neural patterns for MI and ME of different hand actions are specific enough to decode the respective experimental condition based on these patterns. To test whether MI and ME of different action types (aiming, extension–flexion, squeezing) evoked separable response patterns in a given ROI, we conducted a linear discriminant analysis (LDA) with leave-one-run-out cross-validation for each subject using functions from the MATLAB statistics toolbox. We classified activations based on t-contrast images derived from the GLM analysis described above to achieve a down-weighting of noisier voxels (compared with raw beta values; Misaki et al. 2010; Walther et al. 2016).

The *t*-values within an ROI were vectorized for each contrast separately, deriving 3 response vectors per run for both MI and ME. To avoid the influence of potential differences in mean amplitude and variance, we additionally z-scored all t-maps. LDA requires the dimensionality of the data to be lower than the number of training patterns provided. We used principal component analysis (PCA) to reduce the number of features significantly below the number of training samples (we used the first 5 principal components; c.f., Pilgramm et al. 2016) but still capture most of the variance in the data (variance explained ≥60%). Note that the PCA was done across all data and therefore included what would become the test data of individual folds. This does not, however, constitute 'double-dipping' (Kriegeskorte et al. 2009). The PCA was entirely blind to data labels. Therefore, a PCA across all data was possible without 'peeking' for each fold. In each iteration of the cross-validation, these shortened vectors were split into a set of test and training data corresponding to data from 1 and 19 runs, respectively. The LDA algorithm was provided with labels indicating the condition for each of the training examples, and a linear decision hyperplane was derived on the basis of these data. This decision criterion was applied, in turn, to the test data and used to assign condition labels to each of the 3 test vectors.

We compared each of the assigned labels with the veridical labels and counted correct and incorrect assignments as 1 and 0, respectively. The whole procedure was repeated until each run had served as test data once, and we then calculated the proportion of correct assignments across the folds of this cross-validation procedure. This proportion of correct assignments was derived separately for each subject, ROI, and the MI and ME conditions. To test the respective decoding accuracies for significance, we performed a permutation analysis with random labeling of the classes, providing a more robust test of statistical significance than a one-sample *t*-test against chance (Stelzer et al. 2013). In each of 2000 iterations per subject and ROI, the action labels of the 60 data samples were randomly shuffled. The classification accuracy of this randomly labeled data set was calculated using the leave-one-run-out cross-validation approach described above. *P* values were derived as the proportion of random shuffles resulting in an accuracy as high (or higher) than the one observed for the actual (unshuffled) labels, with the smallest possible *P*-value fixed to 0.0005 (Nichols and Holmes 2001). All *P* values were corrected for multiple ROIs using the Holm–Bonferroni method (Holm 1979). Furthermore, we calculated classifier sensitivity (d') for each action type and ROI based on the labels predicted by our classifier.

We used a similar procedure to classify neural activation patterns according to modality (MI or ME). The difference was that we now used all 6 (i.e., imagined and executed) t-contrast images per run and labeled them according to their modality. The statistical significance of the decoding accuracies was determined using permutation analysis, which randomly assigned modality labels to the data in each of 2000 iterations per subject and ROI. Again, *P* values were derived as the probability of getting a value as large as the real-label performance in the randomization distribution and were Holm–Bonferroni corrected.

Searchlight Analysis

In a next step, we performed an additional searchlight analysis (Kriegeskorte et al. 2006; cf. De Haas et al. 2013). This analysis serves as a control analysis in order to test whether and where patterns of neural activity carried information about the content of our different experimental conditions (i.e., the different action types and modalities) outside our prespecified ROIs that belong to the core and broader motor system. For this analysis, we derived activation patterns from the same (trial-specific and z-scored) t-maps that we used for the ROI analysis described above. The searchlight consisted of a sphere with a radius of 5 voxels that was centered on each cortical gray matter voxel for each participant's brain in turn (using FreeSurfer segmentations excluding the cerebellum). For each iteration, the analysis was restricted to the gray matter voxels intersecting the respective searchlight sphere. The corresponding patterns were read out for each trial, and we applied the same classification procedure as described for the ROI analysis. Classification accuracies were projected back onto the seed voxel, resulting in an accuracy map for each participant. We subtracted chance level (1/3) from these accuracy maps, spatially smoothed them with a small Gaussian kernel (FWHM 2 mm), and normalized them to MNI space http://www.loni.ucla.edu/ICBM/. In the imagery condition, we tested for whole-brain family-wise-error (FWE) corrected significance at

cluster level ($P < 0.05$ FWE; voxelwise cluster forming threshold $P < 0.001$ uncorrected). In the execution condition, we tested for whole-brain FWE-corrected significance at voxel level ($P < 0.05$ FWE). Here, we used different thresholds, because the level of neural activity associated with MI is generally lower than that associated with ME. Significant clusters and voxels were identified anatomically using the Juelich Histological Atlas implemented in the SPM Anatomy Toolbox (v. 2.1; http://www.fz-juelich.de/inm/inm1/DE/Forschung/_docs/SPMAnatomyToolbox/SPMAnatomyToolbox_node.html).

Cross-modal Classification

To test whether MI and execution of a specific hand movement share a similar neural code in frontal and parietal motor regions, we attempted a cross-modal classification. In this analysis, we performed the same steps for the LDA classification as described before, but, this time, a classifier trained with the respective 19 execution runs decoded the action types for an imagined run and vice versa. Significant classification accuracies (determined by permutation tests as described above) thus imply a similarity between neural codes for different hand actions across MI and ME.

Representational Similarity Analysis

Further, we employed an RSA analysis in order to characterize the geometry of neural representations in frontal and parietal motor regions for MI and ME of different hand movements. RDMs characterize the pairwise dissimilarity of activation patterns evoked by different action types and modalities.

For this analysis, we used the toolbox from Nili et al. (2014). The t-maps obtained for the imagined and executed hand movements were compared with each other using correlation distance. For each ROI, all pairwise comparisons were assembled in an RDM with (1 – Pearson linear correlation) as the respective degree of dissimilarity leading to a 6 × 6 RDM. The RDMs were calculated separately for each experimental run and averaged for each subject. This yielded 20 brain RDMs (1 per subject) for each of the 16 ROIs. These were used to calculate the noise ceiling and the similarity between model RDMs and each of these single-subject RDMs. Then, we used multidimensional scaling (MDS) to project the high-dimensional RDM space onto 2 dimensions and get a graphical impression of representational distances. For this purpose, the 20 subject RDMs were averaged to obtain a single RDM per ROI.

Computational Models

Finally, we tested several model predictions against these brain RDMs to arbitrate between theoretical stances regarding MI and ME. Specifically, we compared the brain RDMs of the 16 ROIs with 7 different model predictions: a purely modality-based, a purely action type–dependent, and 5 different mixed models. The latter type of models predict a modulation of pattern similarities depending on both, modality and the action types. Examples of these models are shown in Figure 2*b*. The comparison between brain and model RDMs was based on Pearson's linear correlation.

Modality Model

The modality model assumes a categorical distinction between the 2 modalities (i.e., MI and ME) only in the corresponding model RDM, the dissimilarities for all within-modality comparisons are 0 (identical neural response across action types within a modality), and 1 for all between-modality comparisons (totally unrelated neural responses across MI and ME).

Action Type Model

The action type model is also a categorical model. This model assumes a categorical distinction between the 3 action types: squeezing, aiming, and extension–flexion. In this model RDM, the dissimilarities between identical action types were 0 (regardless of modality) and those between different action types were 1 (again, regardless of modality).

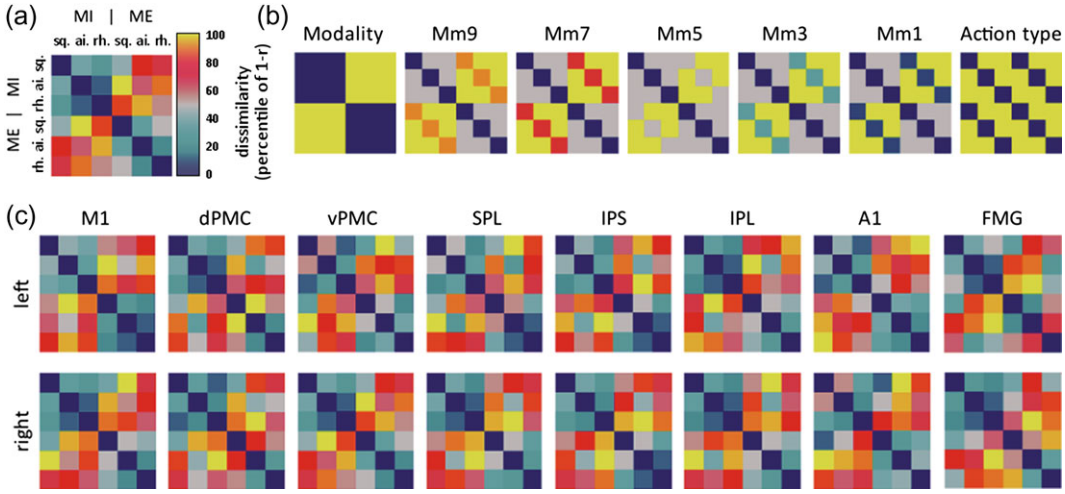

Figure 2. RDMs for models and brain regions. (*a*) Legend showing the arrangement of the 6 experimental conditions (sq. = squeezing, ai. = aiming, rh. = rhythmic extension–flexion) within 1 RDM. The percentiled RDM captures the pairwise dissimilarities between the response patterns elicited by the stimuli. By definition, the RDM is symmetric and has a zero diagonal. Vertical scale illustrating the color coding of the dissimilarity (percentile of 1 – Pearson correlation across space) values. (*b*) RDMs of the theoretical models that assume different similarities of the neural pattern based on modality and action type. The first shows an action modality–based model that assumes equal neural patterns for each action type within an action modality. The last shows an action type–based model that assumes equal neural patterns for a given action type across action modalities. The 3 mixed models in between vary with regard to the degree of functional equivalence they assume between modalities of a given action type. Modality dissimilarity varied between models and was fixed to 0.1 (Mm1), 0.3 (Mm3), 0.5 (Mm5), 0.7 (Mm7), and 0.9 (Mm9), respectively. In all mixed models, the dissimilarity between different action types within 1 modality was fixed to 0.5 and the dissimilarity between different action types of different modalities was fixed to 0. (*c*) RDMs of the brain data for every ROI (means across participants).

Mixed Models

We also tested 5 different mixed models (Mm) that predict a dependency of the observed neural pattern on modality as well as action type. In all models, the dissimilarity between different action "types within a modality" was fixed to 0.5 and the dissimilarity between different action "types across modalities" was fixed to 1. These values matched the brain RDMs within the different ROIs well (correlations for different action types ranged from 0.4 and 0.6 within a modality and between 0 and 0.15 across modalities). The dissimilarity of "identical" action types across modalities (i.e., the dissimilarity of MI and ME for a given action) varied between the defined models and was fixed to 0.1, 0.3, 0.5, 0.7, and 0.9, respectively. These models were designated Mm1, 3, 5, 7, and 9, respectively. Using these models, we tested different degrees of neural similarity between neural patterns elicited by the MI and ME of 1 action type. For example, the Mm9 model assumes a low degree of neural similarity of neural patterns associated with MI and ME.

Pearson Linear Correlation, RDM Relatedness, and Noise Ceiling

To compare brain and model RDMs, we used Pearson linear correlation and one-sided signed-rank test across the single-subject RDM correlations. To test differences between fits across models, we used 2-sided signed-rank tests across subjects for each pair of model RDMs. To account for multiple testing, we controlled the false-discovery rate at 0.05.

The amount of variance, that a model RDM can explain is limited by the variability across subjects. Therefore, an estimation of the noise ceiling is needed to indicate how much variance an ideal model RDM can explain given the noise level. The average of all subject RDMs can be used as an estimate of the ideal model RDM. The average correlation of this average RDM with the 20 subject RDMs provides the upper bound. We estimated the lower bound by applying a leave-one-subject-out approach. We computed and averaged the correlation of each single-subject RDMs with the average RDM of the other 19 subjects, providing the lower bound of the ceiling. A model RDM is deemed to capture the true dissimilarity structure of the brain RDM as well as possible when its correlation reaches the lower bound of the ceiling.

Subjective Rating and EMG Data Acquisition and Analysis

After each trial in the fMRI session, subjects rated the success of each experimental trial on a 7-point Likert scale ranging from very high (7) to very low (1). We calculated mean rating scores for each experimental condition and computed a repeated-measures analysis of variance (ANOVA) to examine the effects of the respective action (aiming, squeezing, rhythmic extension–flexion) or the experimental condition (imagery, execution) on the subjective ratings.

We analyzed EMG data collected in the fMRI session by determining the area under the curve. These data were then averaged for each subject in each condition. The averaged data were subjected to multiple paired *t* tests comparing EMG activity for each imagery condition with EMG activity in the rest condition. All *P* values were corrected for multiple ROIs using the Holm–Bonferroni method (Holm 1979).

Results

Behavioral Data

Subjective Ratings

All subjects gave high ratings in all experimental conditions (mean ratings > 5.2). A repeated-measures ANOVA revealed a significant main effect of modality, $F(1, 19) = 62.568$, $P < 0.001$, $\eta^2 = 0.767$ with higher ratings for ME than MI (Fig. 1c), a significant Modality × Action interaction, $F(2, 38) = 16{,}238$, $P < 0.001$, $\eta^2 = 0.461$ (MI of the aiming movement was rated highest, while it was the action type with the lowest ratings during ME), but no main effect of action, $F(1.23, 23.45) = 1.294$, $P = 0.277$, $\eta^2 = 0.064$.

EMG Data

Muscular activity during MI was controlled during scanning. A repeated-measure ANOVA revealed a significant main effect of experimental condition, $F(2.11, 82.16) = 43.344$, $P < 0.001$, $\eta^2 = 0.526$. Post hoc *t* tests showed no significant difference between all imagery conditions compared with resting baseline but significant differences between the execution of actions and the baseline condition ($P < 0.001$; Bonferroni adjusted). All mean values and standard errors are depicted in Figure 1d.

Neuroimaging Data

Multivariate fMRI Results

To test whether response patterns in a given ROI carried information about the *type* of action, we compared decoding performance in each ROI against chance level separately for both *modalities*. For MI (Fig. 3a), the imagined type of action could be classified significantly above chance level in left M1 ($P < 0.05$), left dPMC ($P < 0.05$), left ($P < 0.01$), and right SPL ($P < 0.05$), as well as right IPS ($P < 0.05$). No significant classification was found for right M1, right dPMC, vPMC, left IPS, IPL, A1, and FMG. For ME (Fig. 3b), the type of action could be classified significantly in left and right M1, left and right dPMC, left and right SPL, left and right IPS, left IPL (all $P < 0.001$), as well as left vPMC ($P < 0.01$), right vPMC ($P < 0.05$), right IPL ($P < 0.01$), and left A1 ($P < 0.05$). No significant classification was found for right A1 and FMG. All *P* values were derived from permutation analyses and were corrected for multiple testing using the Holm–Bonferroni method. In order to test for significant differences between the different decoding accuracies for ME, we performed an 8 × 2 (ROI × hemisphere) repeated-measures ANOVA as well as post hoc multiple pairwise comparisons. The results revealed a significant main effect of ROI [$F(7, 133) = 81.648$, $P < 0.001$, $\eta^2 = 0.811$], a significant main effect of hemisphere [$F(1, 19) = 46.721$, $P < 0.001$, $\eta^2 = 0.711$], and a significant ROI × hemisphere interaction [$F(7, 133) = 5{,}439$, $P < 0.001$, $\eta^2 = 0.223$]. Post hoc pairwise comparison (Holm–Bonferroni corrected) showed that decoding performance in A1 was significantly lower compared with all other ROIs ($P < 0.001$ for M1, dPMC, SPL and IPS; $P < 0.01$ for vPMC and IPL) and did not differ significantly from FMG. As for FMG, the analysis of several further control ROIs revealed no significant decoding (gyrus rectus, transverse frontopolar gyri and sulci, temporal pole, the respective data are not shown due to space constraints). An additional control analysis revealed that significant classification performance was based on classifier sensitivity (d') for all 3 types of actions in both modalities. However, it also revealed an especially high degree of classifier sensitivity for the aiming condition in MI and ME (Fig. 3f,g).

Action modality, that is, whether an action was imagined or executed (Fig. 3e), could be decoded from every single ROI with decoding accuracies ranging from 59.1% to 96.7% ($P < 0.05$; Holm–Bonferroni corrected).

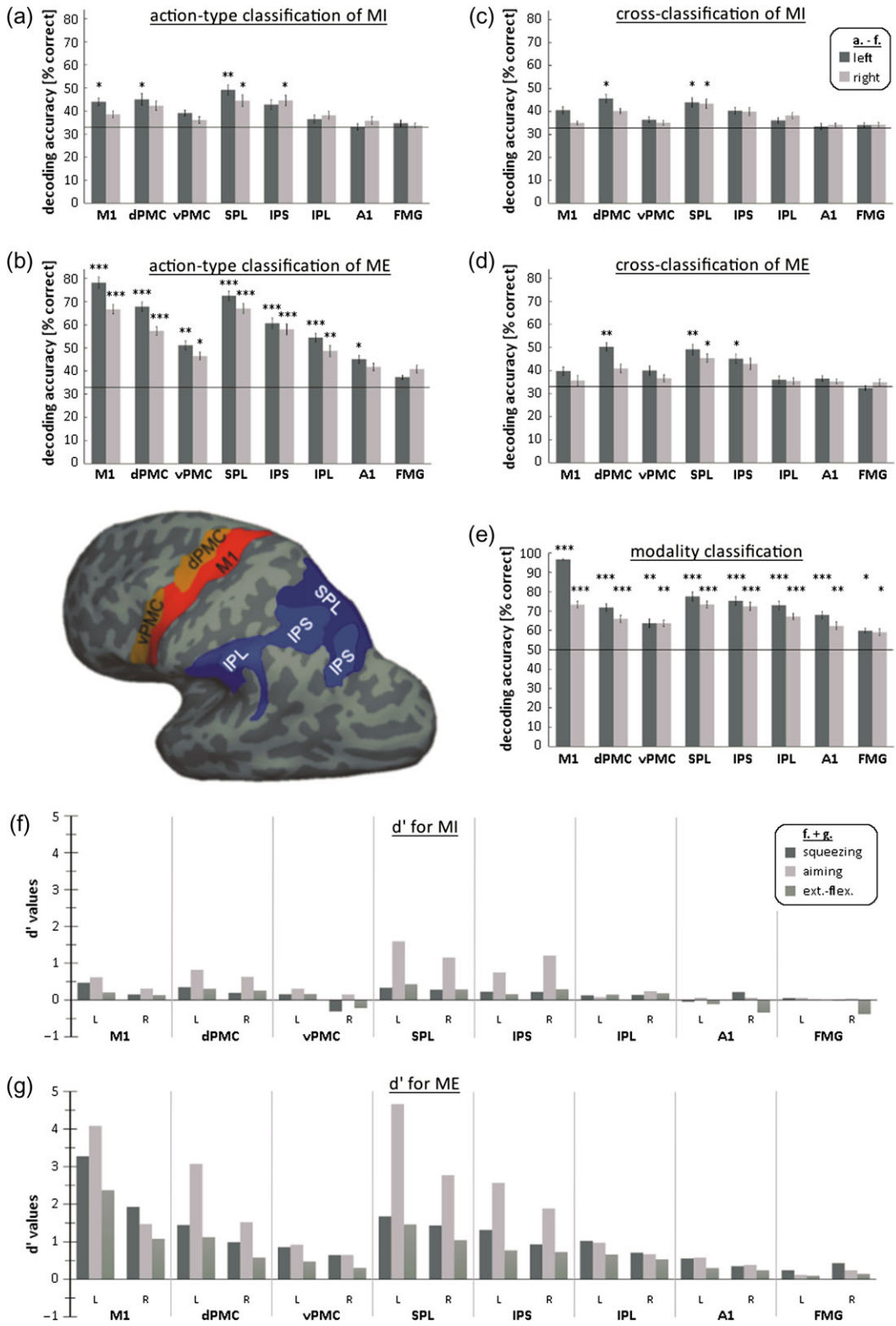

Figure 3. Decoding results for several classifications in every ROI. (*a*) MI decoding results: bars and error bars indicate the mean accuracy (% correct) ±1 standard error of the mean (SEM) with which the type of imagined action could be decoded from activation patterns in a given ROI. (*b*) ME decoding results: bars and error bars indicate the mean accuracy (% correct) ±1 SEM with which the type of executed action could be decoded from activation patterns in a given ROI. (*c*) MI cross-classification: bars and error bars indicate the mean accuracy (% correct) ±1 SEM with which imagined actions in a given ROI could be decoded by a classifier trained with ME data. (*d*) ME cross-classification: bars indicate the mean accuracy (% correct) ±1 SEM with which executed actions in a given ROI could be decoded by a classifier trained with MI data. (*e*) Action modality decoding results: bars indicate the mean accuracy (% correct) ±1 SEM with which the type of action modality could be decoded from activation patterns of the imagined and executed actions in a given ROI. For (*a*) – (*e*): left and right bars for each ROI represent the corresponding areas of the left and right hemisphere, respectively. The black line marks chance level. Asterisks indicate statistical significance determined by permutation analysis, adjusted for

Searchlight Results

We used a searchlight approach in addition to our ROI analyses to explore which regions of the brain carried information about imagined and executed types of hand action (see Methods, above). For MI, this analysis confirmed that imagined hand actions could be decoded from activity patterns within left M1, dPMC, vPMC, preSMA, SPL and IPL, as well as the right M1, dPMC, vPMC, and IPL. Note that most of these areas are within an extended cluster in each hemisphere. In addition, the searchlight analysis revealed significant clusters in right somatosensory cortices (Brodman Area 1 and 2), right Brodman Area 3, and left lateral occipital cortex (Area hOc4la).

For ME, activity patterns could be used to decode executed hand actions in left M1, dPMC, vPMC, posterior supplementary motor area (SMAprop) (all of them in 1 cluster), IPL, and SPL; as well as in right M1, dPMC, IPL, and SPL. In addition, the searchlight analysis revealed significant clusters in left and right somatosensory cortices (BA1, BA2, BA3), visual cortex (including V1, V2, V3A, V3d, V3v, V4v), lateral occipital cortex (hOc4lp), left Area 44, right Area FG1, and in TE 1.1 of both hemispheres. See Table 1 for more details.

Cross-Modal Classification

Both, classification of imagery patterns with a classifier trained with execution patterns and vice versa showed significant decoding accuracies in some of our ROIs. Imagined actions (Fig. 3c) could be decoded with a classifier trained on ME data in left dPMC as well as SPL of both hemispheres (all $P < 0.05$). The results for decoding executed actions with a classifier trained on MI data are similar (Fig. 3d). Significant decoding was found in left dPMC, SPL of both hemispheres (all $P < 0.01$) as well as in right IPS ($P < 0.05$). All P values were derived from permutation analyses and corrected for multiple ROIs using the Holm–Bonferroni method (Holm 1979).

Representational Similarity Analysis

Multidimensional Scaling

Visual inspection using MDS showed a spatial organization of the 6 conditions that was generally the same in every ROI: First, the execution and the imagery conditions were separated into 2 clusters. Second, the geometry of the different action types within the execution and imagery clusters were the same, with specific actions located face to face across modalities (Fig. 4).

Correlations with Model Predictions

Table 2 shows the correlations between model predictions and brain RDMs for different brain regions. This measure reflects how well the response pattern dissimilarities for the several brain regions are explained by the 7 different model RDMs. The action type model RDM did not correlate (Pearson correlation, mean = −0.020) with any brain RDM significantly, but the modality model RDM (Pearson correlation: mean = 0.359), and all 5 mixed models correlated significantly with each brain RDM (mean Pearson correlations for Mm1, 3, 5, 7, and 9 were 0.205, 0.251, 0.300, 0.335, and 0.331, respectively) (Fig. 5).

Considering individual ROIs, the majority of RDMs was best explained by 2 models. The Mm9 model provided the best fit for data in left and right M1, right vPMC, right IPS, left IPL, and left A1. In contrast, the Mm7 model best explained the data in left dPMC, left vPMC, left and right SPL, left IPS, right IPL, and right A1. The difference between the obtained correlations of these 2 models was very small and significant only for left M1 (Fig. 6). These models assume that the correlations between

Table 1 RDM correlations between brain regions and models

ROI	L/R	Ceiling	Correlation to model						
			Modality	Mm9	Mm7	Mm5	Mm3	Mm1	Action type
M1	L	[0.736, 0.764]	0.708****	0.714****	0.663****	0.540****	0.404****	0.290****	−0.205^{ns}
	R	[0.406, 0.485]	0.388****	0.397****	0.380****	0.322****	0.253***	0.193***	−0.080^{ns}
dPMC	L	[0.359, 0.449]	0.213***	0.233***	0.255****	0.248****	0.223****	0.197****	0.042^{ns}
	R	[0.142, 0.295]	**0.166****	**0.186****	**0.212****	**0.213****	0.197****	0.179****	0.057^{ns}
vPMC	L	[0.187, 0.323]	**0.222*****	**0.238*****	**0.252****	**0.237****	0.208****	0.178****	0.019^{ns}
	R	[0.212, 0.344]	**0.286****	**0.296****	**0.292****	**0.255****	0.207****	0.164****	−0.038^{ns}
SPL	L	[0.385, 0.469]	0.330****	0.356****	0.382****	0.364****	0.322****	0.279****	0.042^{ns}
	R	[0.289, 0.396]	**0.311*****	**0.337****	**0.365****	**0.351****	0.313****	0.273****	0.049^{ns}
IPS	L	[0.434, 0.508]	0.376****	0.394****	0.398****	0.357****	0.298****	0.244****	−0.023^{ns}
	R	[0.328, 0.426]	**0.349****	**0.363****	**0.360****	0.317****	0.260****	0.208***	−0.039^{ns}
IPL	L	[0.322, 0.422]	0.300****	0.309****	0.301****	0.260****	0.208****	0.163****	−0.048^{ns}
	R	[0.349, 0.439]	0.300****	0.315****	0.319****	0.288****	0.241****	0.198****	−0.015^{ns}
A1	L	[0.267, 0.381]	**0.296****	**0.308****	**0.307****	**0.272****	0.224****	0.180***	−0.030^{ns}
	R	[0.123, 0.286]	**0.187****	**0.197****	**0.200****	**0.181****	0.152**	0.126**	−0.008^{ns}
FMG	L	[−0.033, 0.201]	**0.134****	**0.141****	**0.143****	**0.129****	**0.108***	**0.089***	**−0.006^{ns}**
	R	[0.102, 0.271]	**0.163*****	**0.168*****	**0.164*****	**0.141*****	**0.113*****	0.088**	−0.028^{ns}

Pearson RDM correlation coefficients between brain regions and models. Significant correlations indicated by asterisks (*ns* = not significant: *$P < 0.05$; **$P < 0.01$; ***$P < 0.001$; ****$P < 0.0001$). Lower and upper bounds of the noise ceiling are stated in brackets. For each brain region, the 2 highest correlations are highlighted. If the correlation is within the ceiling, it is set in bold.

multiple testing using the Holm–Bonferroni method: *$P < 0.05$, **$P < 0.01$, ***$P < 0.001$. (*f*) MI classifier sensitivity: bars indicate d' values for each action type and ROI based on the labels predicted by our classifier with MI data. (*g*) ME classifier sensitivity: bars indicate d' values for each action type and ROI based on the labels predicted by our classifier with ME data. For (*f*) + (*g*): the 3 bars for each ROI represent the corresponding hand movements (squeezing, aiming, and extension–flexion). The brain picture shows the anatomical location of ROI labels on the reconstructed surface of an example hemisphere.

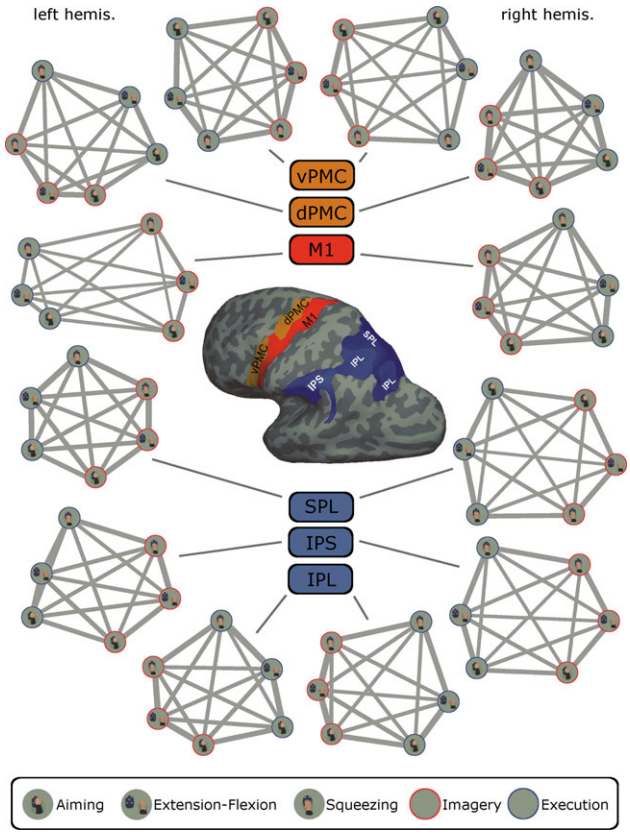

Figure 4. MDS plots of brain RDMs. For each ROI, an MDS plot (minimizing metric stress) shows the similarities of the neural pattern elicited by the 6 experimental conditions. The closer images are to each other, the more similar their neural patterns. By arranging this higher dimensional similarity structure into 2D, the effective distances between the neural patterns get inevitably distorted. This deviation is indicated by a gray connection line, which, like a rubber band, becomes thinner when stretched beyond the length that would exactly reflect the dissimilarity it represents, respectively, becomes thicker when compressed. The thickness of each line is chosen such that the area of each connection line (length time thickness) precisely reflects the undistorted similarity measure. Each MDS plot visualizes the respective brain RDM in Figure 2c. The brain in the middle shows the anatomical location of ROI labels on the reconstructed surface of an example hemisphere.

executed and imagined action types are relatively low, compared with pattern correlations due to shared modality. Thus, for a large part of our ROIs, pattern similarity was driven by modality to a greater degree than action type. The highest correlation between MI- and ME-evoked patterns for different hand actions was found in right dPMC, which was best explained by the Mm5 model, indicating that this region showed a higher degree of neural similarity between MI and ME. Furthermore, the model data revealed that MI- and ME-evoked patterns correlated in a range of 0.3–0.5 in dPMC and SPL (which is in line with the Mm5 and Mm7 predictions), while all other ROIs showed lower. This is illustrated in Figure 6. The figure gives a brief overview of the 2 highest correlating models for each ROI as well as of the statistical model fit. For further information see supplemental table S1.

Despite moderate absolute correlation values, the best fitting model predictions for a number of ROIs reached the noise ceiling. This indicates these performed as well as possible, given the variability of the data. For example, the modality model was able to explain the data in right dPMC, left and right vPMC, right SPL, right IPS, and left and right A1. The Mm9 and Mm7 models reached the ceiling in the same ROIs. Almost the same results (the same ROIs except for the right IPS) were observed for the Mm5 model. Furthermore, all mixed models reached the noise ceiling for vPMC and A1 in both hemispheres. In summary, the mixed models performed best in most ROIs and reached the noise ceiling in a number of them, indicating a low-to-moderate similarity of MI and ME representations within these motor regions.

Discussion

It has been proposed that MI is a simulation based on own motor representations that are also used while executing an action (Jeannerod 2001; Grush 2004). This led to the assumption of a so-called functional equivalence between imagining and executing an action. This study used a multivariate fMRI approach to investigate the functional organization of MI and ME in different motor regions. Participants imagined and executed 3 different hand actions of the right hand (aiming, extension–flexion, and squeezing). The respective fMRI data were then fed into a battery of multivariate analysis approaches.

Our findings show that for MI, the type of action could be classified significantly above chance level in the left and right M1, left PMC, left and right dPMC, left vPMC, left and right PPC, left and right SPL, left and right IPS, and right IPL. For ME, the respective type of action could be classified significantly in every ROI, except right A1 and FMG of both hemispheres. The modality of actions could be classified significantly above chance level in every ROI. Surprisingly, decoding of ME action types was possible in left A1 although the decoding accuracy was significant lower compared with those in all motor regions and decoding did not work in FMG, our nonsensory control region. Here, we can only speculate about the source of the effect in left A1. One possible explanation is multisensory feedback processes during the execution of specific movements. Within this framework, Vetter et al. (2014) argue that sensory priors can be transmitted between sensory modalities and through cortical feedback from higher areas, in order to prepare early sensory areas with a predictive model for incoming external information.

These results replicate previous findings showing that patterns of activity within motor, premotor, and posterior parietal regions differentiate between, first, different types of hand actions (Pilgramm et al. 2016) and second, between action modalities (Filimon et al. 2015; Park et al. 2015). This suggests that frontal as well as parietal motor-related areas represent the content as well as the modality of imagined and executed actions. Furthermore, these results showed that cross-classification succeeded for MI in left dPMC and SPL of both hemispheres. For ME, cross-classification succeeded in left dPMC, SPL of both hemispheres as well as in left IPS. This demonstrates that there is at least some similarity between MI- and ME-induced neural patterns for specific hand actions in broad areas of the human motor system. Therefore, the results stand for some degree of consistency between neural codes for MI and ME within these regions. However, the relatively low values of the cross-classification, the successful decoding of modality, and the testing of model predictions (see below) demonstrates that the neural codes for MI and ME are clearly distinct at the same time.

To gain some notion of the degree of similarity and consistency of neural patterns induced by MI and ME in different motor regions, we characterized the representations in different frontal and parietal motor regions by RDMs constructed

Table 2 Searchlight results

	Left/right	Cluster size	MNI coordinates of maximum *t* value			Maximum *t* value
			x	y	z	
MI						
vPMC / dPMC / preSMA / BA4p / BA4a / SPL (7 A/7PC)	L	1852	−15	−55	56	7.36
dPMC / vPMC / BA4p / BA4a / BA1 / BA2	R	1093	42	−31	59	7.16
SPL (5 Ci)	L	10	−15	−37	41	5.76
IPL (PGp)	R	41	33	−82	17	5.60
IPL (Pga)	L	8	−54	−55	32	5.04
IPL (PFcm)	L	54	−48	−40	17	4.86
hOc4la	L	36	−36	−76	8	5.19
Area 33	R	14	6	29	17	4.23
ME						
BA2	R	5	33	−43	56	9.32
BA3b	L	5	−60	−7	29	9.16
BA3b / BA1	L	9	−51	−19	50	12.51
BA3b / BA4a / BA4p	R	151	39	−19	47	11.72
BA3b / BA4a / BA4p / dPMC / vPMC / SMAprop	L	239	−48	−13	32	13.66
dPMC	R	39	39	−10	59	11.50
dPMC	L	8	−30	−19	68	10.27
dPMC	L	7	−12	−10	68	8.56
IPL (PFcm)	R	3	48	−34	17	8.55
IPL (PFt)	R	23	57	−25	41	10.06
IPL (PFt)	L	3	−54	−34	38	8.78
SPL (5 M)	L	99	−15	−40	50	10.28
V1 (hOc1)	R	70	9	−91	−4	11.34
V1 (hOc1)	R	20	6	−85	5	10.24
V1 (hOc1)	L	4	−9	−61	2	9.96
V1 (hOc1)	R	14	6	−79	−4	9.27
V1 (hOc1)	R	4	15	−67	8	8.60
V1 (hOc1)	R	5	15	−67	−1	8.56
V2 (hOc2)	R	16	27	−97	−7	10.09
V2 (hOc2)	L	3	−3	−97	11	8.64
V2 / V3d / V3v	L	154	−6	−82	−7	12.10
V3A (hOc4d)	R	10	18	−85	38	10.83
V3d (hOc3d)	R	10	9	−82	35	8.79
V3d (hOc3d)	L	10	−6	−85	23	9.03
V3d (hOc3d)	R	4	15	−91	23	8.76
V3v (hOc3v)	R	6	30	−85	−13	10.07
V3v (hOc3v)	R	6	15	−76	−7	9.25
V3v (hOc3v)	L	6	−9	−70	−4	8.06
Area 44	L	27	−48	11	5	9.07
Area 5 L (SPL)	R	14	21	−49	62	8.91
Area FG1	R	3	33	−67	−10	7.60
Area hOc4v [V4(v)]	L	3	−33	−79	−16	8.29
Area TE 1.1	L	9	−42	−22	5	9.51
Area TE 1.1	R	6	42	−22	8	8.70
Area hOc4lp	R	5	39	−85	8	11.69
Area hOc4lp	L	3	−33	−82	11	8.47
Area hOc4lp	L	4	−30	−94	−7	8.43

Clusters with above chance decoding of action type in MI condition. Voxels with above chance decoding action types in ME condition. MI: $P < 0.05$, whole-brain FWE-corrected on cluster level. ME: $P < 0.05$, whole-brain FWE-corrected.

from fMRI patterns for different types of imagined and executed hand actions. The RDMs of different motor and motor-related areas were highly similar to each other with respect to their general representational geometries of executed and imagined actions. In all tested regions, the neural pattern of MI and ME conditions were underpinned quite distinctly by 2 separated clusters in the respective MDS. However, we also found that the geometry of the different hand movements for the execution and imagery was the same in every MDS. Hence, the neural organization of action types was similar across imagery and execution. With respect to the tested model predictions, we found the best fits for the representational geometries of mixed models indicating that neural representations have both common and distinct components across modalities. For nearly all tested ROIs, the best model fit was found for the mixed models assuming a relatively low-to-moderate degree of similarity between the neural patterns

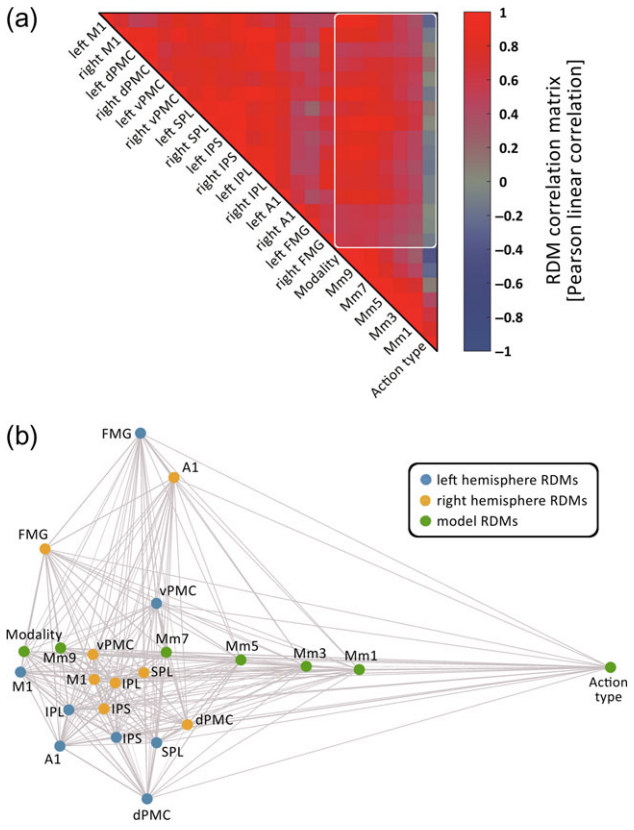

Figure 5. Visualizing relationships among model and brain RDMs. (*a*) Matrix of all model and brain RDM correlations. Each entry compares 2 RDMs by Pearson linear correlation. RDM correlations between brain regions and models are framed. (*b*) MDS (minimizing metric stress) of brain and model RDMs. Each point represents an RDM, and distances between the points approximate the dissimilarity (1 – Pearson linear correlation) of the respective RDMs (left and right hemisphere RDMs and model RDMs shown in blue, yellow, and green, respectively).

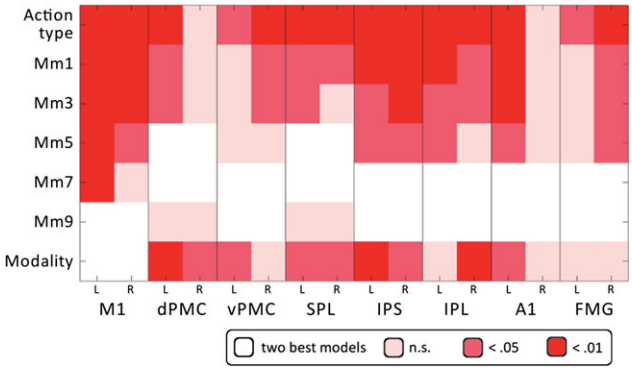

Figure 6. Visualizing differences between RDM model correlations. For each ROI, the 2 models with the highest RDM correlation (white background) are shown. Furthermore, significant differences (2-sided signed-rank test across subjects, controlling FDR at 0.05.) with respect to the model fit are shown and indicated by color. Action modality: a purely action modality–based model that assumes equal neural patterns for each action type within an action modality, action type: a purely action type–based model that assumes equal neural patterns for a given action type across action modalities. Mm9/Mm7/Mm5/Mm3/Mm1: mixed models vary with regard to the degree of functional equivalence they assume between action modalities for a given action type and is fixed to 0.9, 0.7, 0.5, 0.3, and 0.1 respectively. Dissimilarity between different action types within a modality was fixed to 0.5; dissimilarity between different action types of different action modalities was fixed to 1.

associated with MI and ME. The exception was in the dorsal premotor sections as well as within the superior parietal cortex. Here, we found the best model fit for the mixed model that assumes a slightly higher similarity between MI and ME.

Our results therefore suggest the following main conclusions: (1) Evoked patterns of neural activity vary systematically according to which type of action is being imagined or executed using the same effector. Thus, frontal as well as parietal motor-related areas represent the content of MI and action execution as well as their modality (Filimon et al. 2015; Park et al. 2015; Pilgramm et al. 2016). (2) ME and MI generate neural patterns that have some degree of consistency as demonstrated by the cross-modal classification. (3) The representational similarity of MI and ME can be considered as low to moderate. (4) The dPMC and the SPL come closest to a 'common code' for MI and ME, showing the highest degree of representational similarity between MI and ME. These results complement and extend previous research by directly comparing MI- and ME-evoked patterns of neural activity and their representational geometry.

dPMC and SPL Showing Greater Similarity Between ME and MI Representations

Generally, the dorsal premotor and superior parietal cortices are considered to be involved in motor preparation processes (Rizzolatti and Sinigaglia 2010). Regarding their anatomical relatedness, it has been confirmed that most parietal input to the dorsal premotor cortex originates from the superior parietal cortex (Wise et al. 1997). The premotor region is involved in many higher level aspects of movement planning such as the preparation and organization of movements and actions (Wise 1985; Rizzolatti and Luppino 2001) or processes such as serial prediction (Schubotz 2007). In particular, the dorsal section of the premotor region is crucial for deciding which action to perform. Furthermore, Cisek and Kalaska (2004) have argued that the activation of dorsal premotor cells is associated with mental rehearsal processes of sensory events and motor tasks. The PPC has been considered to be important for movement intention, decision making, as well as sensorimotor transformation (Andersen 1987; Kalaska et al. 1997; Rizzolatti et al. 1997; Graziano and Gross 1998; Andersen and Buneo 2002; Bueno et al. 2002; Desmurget et al. 2009), and a broad body of literature relates the process of body state estimation to the PPC (Desmurget et al. 2009). A further functional issue of the SPL is the storage of internal models and action representations that are mandatory for action prediction (Winstein et al. 1997; Wolpert et al. 1998a ; Miall 2003; Rizzolatti and Matelli 2003). For example, Aflalo et al. (2015) demonstrated that MI of movements with different goals and trajectories could be decoded from neural populations within the human PPC of a tetraplegic subject. In a recent study, we found that decoding of MI of different actions is possible, especially within the dorsal section of the premotor area and the superior section of the PPC. This suggests that both regions carry information regarding the type of an imagined action (Pilgramm et al. 2016). Additionally, these data suggest that these regions show a greater similarity between MI- and ME-evoked patterns than other motor areas. Thus, especially the activity within the dorsal section of the premotor area, which is assumed to decide which kind of action is to be performed (Hoshi and Tanji 2007), shows a relatively high degree of functional equivalence between MI and ME. The same may be the case for the superior section of the PPC, because this region is considered to store internal action models and an internal representation of the body's state

(Wolpert et al. 1998). Both aspects might be mandatory for both MI and ME. The PPC/SPL and the dorsal section of the PMC might especially represent high-level aspects of action (Fogassi and Luppino 2005). One conclusion for the similarity of executed and imagined actions therefore might be that that the similarity of MI and ME is highest for higher levels of action processing like the planning of a movement.

Conclusion

There is a large body of neuroimaging literature concluding that MI and ME depend on equivalent motor representations, because they tend to come with similar activation foci. Newer approaches using multivariate methods, however, argue that it is not the overall activity within motor regions but the distributed activation patterns within them that are critical for the representation of actions, modalities, and action types. This study investigated whether the imagery or execution of 3 different hand actions is accompanied by similar patterns of neural activation in the human core and broader motor regions. Our findings are in line with previous results showing that decoding of both the action content and the action modality is possible for frontal and parietal motor regions (see also Filimon et al. 2015; Park et al. 2015; Pilgramm et al. 2016). This speaks for a distinctiveness of the neural codes underlying MI and ME of different action types. However, they go beyond these previous findings by demonstrating that the neural patterns elicited by the execution or imagery of different action types also resemble each other—as demonstrated by the possibility of cross-classification. They further show that ME and MI share a similar representational geometry for different action types—as indicated by the RSA analysis. A comparison of the data with a range of models indicates that ME and MI representations are neither purely distinct nor purely equivalent. They are best captured by models assuming that ME and MI are distinguishable from each other while preserving a low-to-moderate degree of similarity. Finally, we found the closest similarity of MI- and ME-induced neural activation patterns within the SPL and the dPMC. Both cortical sites are discussed as representing action ideas and internal action models. It appears that the similarity between MI and ME is highest on this level of action ideas and action plans.

Limitations and Open Questions

We find moderate similarities between MI and ME in several frontal and parietal motor areas with higher degrees of similarity for the dPMC and the SPL. However, these data should be interpreted with caution, because fMRI data are indirect measures of neural activation with relatively coarse temporal and spatial resolution. They are further subject to substantial measurement noise as well as potential intersubject and intrasubject variation (indicated by the relatively low noise ceiling in many of our ROIs; cf. Table 2). This variation might be caused by the differences of quality (i.e., vividness) of imagery as well as by differences with respect to the used imagery strategy. For example, subjects might have focused on either more visual or kinesthetic aspects of the imagined movements what is related with different neural activation pattern (Stinear et al. 2006; Guillot et al. 2009). Furthermore, it should be noted that this study investigated MI and ME of 3 hand movements that differ with respect to their transitivity, timing, and goal-directedness. These movement–immanent differences are accompanied by specific neural differences within premotor and parietal areas (cf. Lorey et al. 2014), potentially leading to differential classifier performance for different action types across different areas. In fact, an additional control analysis revealed that significant classification performance was based on classifier sensitivity (d') for all 3 types of actions in both ME and MI. However, it also revealed an especially high degree of classifier sensitivity for the aiming condition in both MI and ME, which was most pronounced in superior parietal cortex. This might be related to the importance of spatial processing for this type of action, but given our limited set of actions definitive conclusion will have to await further research. Against this background, a more systematic investigation of different movement features and their representations in motor regions might be an important future research issue. A third possible limitation might emerge from the fact that MI was performed with eyes closed and ME was performed with eyes open and thus accompanied by processing visual input. This might lead to an underestimation of similarity between MI and ME in regions modulated by visual input (e.g., parietal cortex). However, this difference between conditions ensures that the observed similarity between MI and ME within core and broader motor regions (as shown by the cross-decoding as well as by the representational geometry of the RDMs) is due to motor rather than visual commonalities of MI and ME.

Future studies should explore whether subject variables such as the vividness of imagery or different imagery strategies modulate decoding performance and the similarity between MI and ME. Furthermore, it might be interesting to examine whether the similarity of neural representations is adaptive to the individual motor experience.

Supplementary Material

Supplementary material can be found at: http://www.cercor.oxfordjournals.org/.

Funding

A.Z. is a member of the International Training Group "The Brain in Action" (IRTG 1901) supported by the German Research Foundation (DFG). B.d.H. was supported by a DFG research fellowship (HA 7574/1-1).

Notes

The authors thank Carlo Blecker for his helpful support. We also thank Jonathan Harrow for native-speaker advice. *Conflict of Interest*: None declared.

References

Aflalo T, Kellis S, Klaes C, Lee B, Shi Y, Pejsa K, Shanfield K, Hayes-Jackson S, Aisen M, Heck C, et al. 2015. Decoding motor imagery from the posterior parietal cortex of a tetraplecig human. Science. 348:906–910.

Andersen RA. 1987. The role of inferior parietal lobule in spatial perception and visual-motor integration. In: Plum F, Mountcastle V, Geiger S, editors. Handbook of physiology. Section 1: the nervous system. Volume V. Bethesda (MD): American Physiological Society. p. 483–518Higher Functions of the Brain.

Andersen RA, Buneo CA. 2002. Intentional maps in posterior parietal cortex. Annu Rev Neurosci. 25:189–220.

Buneo C a, Jarvis MR, Batista AP, Andersen RA. 2002. Direct visuomotor transformations for reaching. Nature. 416: 632–636.

Cisek P, Kalaska JF. 2004. Neural correlates of mental rehearsal in dorsal premotor cortex. Nature. 431:993–996.

De Haas B, Schwarzkopf DS, Urner M, Rees G. 2013. Auditory modulation of visual stimulus encoding in human retinotopic cortex. Neuroimage. 70:258–267.

Decety J, Perani D, Jeannerod M, Bettinardi V, Tadary B, Woods R, Mazziotta JC, Fazio F. 1994. Mapping motor representations with positron emission tomography. Nature. 371:600–602.

Deiber MP, Ibañez V, Sadato N, Hallett M. 1996. Cerebral structures participating in motor preparation in humans: a positron emission tomography study. J Neurophysiol. 75:233–247.

Desmurget M, Reilly Karen T, Richard N, Szathmari A, Mottolese C, Sirigu A. 2009. Movement intention after parietal cortex stimulation in humans. Science. 324:811–813.

Destrieux C, Fischl B, Dale A, Halgren E. 2010. Automatic parcellation of human cortical gyri and sulci using standard anatomical nomenclature. Neuroimage. 53:1–15.

Ehrsson HH, Geyer S, Naito E. 2003. Imagery of voluntary movement of fingers, toes, and tongue activates corresponding body-part-specific motor representations. J Neurophysiol. 90:3304–3316.

Filimon F, Rieth C a., Sereno MI, Cottrell GW. 2015. Observed, executed, and imagined action representations can be decoded from ventral and dorsal areas. Cereb Cortex. 25: 3144–3158.

Fogassi L, Luppino G. 2005. Motor functions of the parietal lobe. Curr Opin Neurobiol. 15:626–631.

Friston KJ, Frith CD, Frackowiak RS, Turner R. 1995. Characterizing dynamic brain responses with fMRI: a multivariate approach. Neuroimage. 2:166–172.

Gallivan JP, McLean DA, Flanagan JR, Culham JC. 2013. Where one hand meets the other: limb-specific and action-dependent movement plans decoded from preparatory signals in single human frontoparietal brain areas. J Neurosci. 33:1991–2008.

Gallivan JP, McLean DA, Valyear KF, Pettypiece CE, Culham JC. 2011a. Decoding action intentions from preparatory brain activity in human parieto-frontal networks. J Neurosci. 31: 17149–17168.

Gallivan JP, McLean DA, Valyear KF, Pettypiece CE, Culham JC. 2011b. Decoding action intentions from preparatory brain activity in human parieto-frontal networks. J Neurosci. 31: 9599–9610.

Graziano MSA, Gross CG. 1998. Spatial maps for the control of movement. Curr Opin Neurobiol. 8:195–201.

Grèzes J, Decety J. 2001. Functional anatomy of execution, mental simulation, observation, and verb generation of actions: a meta-analysis. Hum Brain Mapp. 12:1–19.

Grush R. 2004. The emulation theory of representation: Motor control, imagery, and perception. Behav. Brain Res. 27: 377–442.

Guillot A, Collet C, Nguyen VA, Malouin F, Richards C, Doyon J. 2008. Functional neuroanatomical networks associated with expertise in motor imagery. Neuroimage. 41:1471–1483.

Guillot A, Collet C, Nguyen VA, Malouin F, Richards C, Doyon J. 2009. Brain activity during visual versus kinesthetic imagery: an fMRI study. Hum Brain Mapp. 30:2157–2172.

Hanakawa T, Dimyan MA, Hallett M. 2008. Motor planning, imagery, and execution in the distributed motor network: a time-course study with functional MRI. Cereb Cortex. 18: 2775–2788.

Haxby J V, Gobbini MI, Furey ML, Ishai A, Schouten JL, Pietrini P. 2001. Distributed and overlapping representations of faces and objects in ventral temporal cortex. Science. 293: 2425–2430.

Haynes J-D, Rees G. 2005. Predicting the orientation of invisible stimuli from activity in human primary visual cortex. Nat Neurosci. 8:686–691.

Heed T, Beurze SM, Toni I, Roder B, Medendorp WP. 2011. Functional rather than effector-specific organization of human posterior parietal cortex. J Neurosci. 31:3066–3076.

Holm S. 1979. A simple sequentially rejective multiple. Test Procedure. Scand J Stat. 6:65–70.

Hoshi E, Tanji J. 2007. Distinctions between dorsal and ventral premotor areas: anatomical connectivity and functional properties. Curr Opin Neurobiol. 17:234–242.

Hutton C, Bork A, Josephs O, Deichmann R, Ashburner J, Turner R. 2002. Image distortion correction in fMRI: a quantitative evaluation. Neuroimage. 16:217–240.

Jeannerod M. 2001. Neural simulation of action: a unifying mechanism for motor cognition. Neuroimage. 14:S103–S109.

Jeannerod M, Frak V. 1999. Mental imaging of motor activity in humans. Curr Opin Neurobiol. 9:735–739.

Kalaska JF, Scott SH, Cisek P, Sergio LE. 1997. Cortical control of reaching movements. Curr Opin Neurobiol. 7:849–859.

Kamitani Y, Tong F. 2005. Decoding the visual and subjective contents of the human brain. Nat Neurosci. 8:679–685.

Khaligh-Razavi SM, Kriegeskorte N. 2014. Deep supervised, but not unsupervised, models may explain IT cortical representation. PLoS Comput Biol. 10:1–29.

Kriegeskorte N. 2009. Relating population-code representations between man, monkey, and computational models. Front Neurosci. 3:363–373.

Kriegeskorte N. 2011. Pattern-information analysis: From stimulus decoding to computational-model testing. NeuroImage. 56:411–421.

Kriegeskorte N, Goebel R, Bandettini P. 2006. Information-based functional brain mapping. Proc Natl Acad Sci U S A. 103: 3863–3868.

Kriegeskorte N, Kievit RA. 2013. Representational geometry: integrating cognition, computation, and the brain. Trends Cogn Sci. 17:401–412.

Kriegeskorte N, Mur M, Bandettini P. 2008. Representational similarity analysis—connecting the branches of systems neuroscience. Front Syst Neurosci. 2:4, doi: 10.1093/cercor/bhv136.

Kriegeskorte N, Simmons WK, Bellgowan PSF, Baker CI. 2009. Circular analysis in systems neuroscience: the dangers of double dipping. Nat Neurosci. 12:535–540.

Lorey B, Naumann T, Pilgramm S, Petermann C, Bischoff M, Zentgraf K, Stark R, Vaitl D, Munzert J. 2013. How equivalent are the action execution, imagery, and observation of intransitive movements? Revisiting the concept of somatotopy during action simulation. Brain Cogn. 81:139–150.

Lorey B, Naumann T, Pilgramm S, Petermann C, Bischoff M, Zentgraf K, Stark R, Vaitl D, Munzert J. 2014. Neural simulation of actions: effector-versus action-specific motor maps within the human premotor and posterior parietal area? Hum Brain Mapp. 35:1212–1225.

Lotze M, Montoya P, Erb M, Hulsmann E, Flor H, Klose U, Birbaumer N, Grodd W. 1999. Activation of cortical and cerebellar motor areas during executed and imagined hand movements: an fMRI study. J Cogn Neurosci. 11: 491–501.

Miall RC. 2003. Connecting mirror neurons and forward models. Neuroreport. 14:2135–2137.

Misaki M, Kim Y, Bandettini PA, Kriegeskorte N. 2010. Comparison of multivariate classifiers and response normalizations for pattern-information fMRI. Neuroimage. 53:103–118.

Munzert J, Lorey B, Zentgraf K. 2009. Cognitive motor processes: the role of motor imagery in the study of motor representations. Brain Res Rev. 60:306–326.

Nichols TE, Holmes AP. 2001. Nonparametric permutation tests for functional neuroimaging: a primer with examples. Hum Brain Mapp. 15:1–25.

Nili H, Wingfield C, Walther A, Su L, Marslen-Wilson W, Kriegeskorte N. 2014. A toolbox for representational similarity analysis. PLoS Comput Biol. 10:1–11.

Oosterhof NN, Tipper SP, Downing PE. 2012a. Visuo-motor imagery of specific manual actions: a multi-variate pattern analysis fMRI study. Neuroimage. 63:262–271.

Oosterhof NN, Tipper SP, Downing PE. 2012b. Viewpoint (in) dependence of action representations: an MVPA study. J Cogn Neurosci. 24:975–989.

Park CH, Chang WH, Lee M, Kwon GH, Kim L, Kim ST, Kim YH. 2015. Which motor cortical region best predicts imagined movement? Neuroimage. 113:101–110.

Pilgramm S, de Haas B, Helm F, Zentgraf K, Stark R, Munzert J, Krüger B. 2016. Motor imagery of hand actions: Decoding the content of motor imagery from brain activity in frontal and parietal motor areas. Hum Brain Mapp. 37:81–93.

Porro CA, Francescato MP, Cettolo V, Diamond ME, Baraldi P, Zuiani C, Bazzocchi M, diPrampero PE. 1996. Primary motor and sensory cortex activation during motor performance and motor imagery: A functional magnetic resonance imaging study. J Neurosci. 16:7688–7698.

Rizzolatti G, Fogassi L, Gallese V. 1997. Parietal cortex: from sight to action. Curr Opin Neurobiol. 7:562–567.

Rizzolatti G, Luppino G. 2001. The cortical motor system. Neuron. 31:889–901.

Rizzolatti G, Matelli M. 2003. Two different streams form the dorsal visual system: anatomy and functions. Exp Brain Res. 153:146–157.

Rizzolatti G, Sinigaglia C. 2010. The functional role of the parieto-frontal mirror circuit: interpretations and misinterpretations. Nat Rev Neurosci. 11:264–274.

Schubotz RI. 2007. Prediction of external events with our motor system: towards a new framework. Trends Cogn Sci. 11:211–218.

Shapleske J, Rossell SL, Woodruff PW, David AS. 1999. The planum temporale: a systematic, quantitative review of its structural, functional and clinical significance. Brain Res Brain Res Rev. 29:26–49.

Stelzer J, Chen Y, Turner R. 2013. Statistical inference and multiple testing correction in classification-based multi-voxel pattern analysis (MVPA): random permutations and cluster size control. Neuroimage. 65:69–82.

Stephan KM, Fink GR, Passingham RE, Silbersweig D, Ceballosbaumann AO, Frith CD, Frackowiak RSJ. 1995. Functional anatomy of the mental representation of upper extremity movements in healthy subjects. J Neurophysiol. 73:373–386.

Stinear CM, Byblow WD, Steyvers M, Levin O, Swinnen SP. 2006. Kinesthetic, but not visual, motor imagery modulates corticomotor excitability. Exp Brain Res. 168:157–164.

Vetter P, Smith FW, Muckli L. 2014. Decoding sound and imagery content in early visual cortex. Curr Biol. 24:1256–1262.

Walther A, Nili H, Ejaz N, Alink A, Kriegeskorte N, Diedrichsen J. 2016. Reliability of dissimilarity measures for multi-voxel pattern analysis. Neuroimage. 137:188–200.

Winstein CJ, Grafton ST, Pohl PS. 1997. Motor task difficulty and brain activity: Investigation of goal- directed reciprocal aiming using positron emission tomography. J Neurophysiol. 77: 1581–1594.

Wise SP. 1985. The primate premotor cortex: past, present, and preparatory. Annu Rev Neurosci. 8:1–19.

Wise SP, Boussaoud D, Johnson PB, Caminiti R. 1997. Premotor and parietal cortex: corticocortical connectivity and combinatorial computations. Annu Rev Neurosci. 20:25–42.

Wolpert DM, Goodbody SJ, Husain M. 1998. Maintaining internal representations: the role of the human superior parietal lobe. Nat Neurosci. 1:529–533.